Quad-element LTE hidden car roof antenna system

Yousaf, Irfan; Aliakbari Abar, Hanieh; Lau, Buon Kiong

Published in:
IEEE Antennas and Wireless Propagation Letters

DOI:
10.1109/LAWP.2023.3303337

2023

Document Version:
Peer reviewed version (aka post-print)

IEEE AWPL Focused Cluster on Recent Advances in Applications Involving Mutual Coupling (accepted version)

Quad-element LTE Hidden Car Roof Antenna System

Irfan Mehmood Yousaf, Hanieh Aliakbari, *Graduate Student Member, IEEE*, and Buon Kiong Lau, *Fellow, IEEE*

***Abstract*—This work presents the systematic design and optimization of a compact quad-element MIMO antenna system in a roof cavity for the expected channel behavior at a 700 MHz LTE band. Beginning with a standard low-profile antenna element, the desired radiation pattern is synthesized by structural modification. The configuration for a quad-element design is then optimized. The results show that the proposed hidden solution even outperforms a non-hidden reference antenna of four quarterwave-monopoles in the cavity, making it attractive for real application.**

***Index Terms*— MIMO systems, vehicular antenna, monopole antennas, hidden antenna, multiplexing efficiency.**

I. Introduction

The new trend of "connected cars" puts higher data rate requirement on vehicles, calling for more than two antennas to be used for MIMO operation [1]. At the same time, the automotive industry is looking for hidden antenna solution due to design and styling preferences as well as increasing trend of panorama glass roof.

One common approach to designing a hidden antenna is to place a low-profile antenna in a cavity formed on the car roof. To reliably receive LTE base station signals, the antenna should have good gain just above the horizon (i.e., monopole-like patterns). There are low-profile vehicular MIMO antennas with monopole-like radiation patterns for low LTE bands [2]-[4]. However, these MIMO antennas have only two elements, and since they were developed for the non-hidden "shark-fin" module, their overall profiles are still quite high, e.g., 60-73 mm [2]-[4]. Moreover, with the shark-fin module already congested with antennas for many other services, e.g., FM, GPS, Wireless LAN, there is no space for adding two more ports for a quad-element design. Therefore, hiding the antenna in a suitably dimensioned low-profile roof cavity also provides greater design flexibility, with one example being the hidden Telematics and Connectivity Unit (TCU) under the glass roof of Volvo EX90.

There have been recent investigations on the design and performance of hidden vehicular antennas in roof cavities, e.g., [5]-[9]. However, they focus on single-element antennas and only a few papers consider a low LTE band (e.g., Band 13, 746-787 MHz) [7]-[9]. At the lower end of common LTE bands, Band 13 poses a great challenge when it comes to designing a physically compact antenna that can fit into the roof cavity. Moreover, due to lower propagation loss at the low band, it is commonly used to ensure good coverage. Therefore, it is both practically important and challenging to design and optimize compact MIMO antennas of beyond two elements inside a roof cavity for the low LTE band that can facilitate good MIMO performance for the expected usage environment.

Furthermore, the interest in the low band is motivated by the size of the MIMO antenna or telematics module being dictated by the antenna's lowest operating frequency, due to the size of the antenna element and the distance between the elements for good MIMO performance. If the overall structure is optimized for the lowest frequency, good performance could also be expected in higher frequencies because of the larger electrical distances between the elements. Moreover, if separate elements are used for the higher frequencies, then more elements can instead be utilized for the same element distance [10].

In this work, we present a comprehensive design approach for a quad-element MIMO antenna in a roof cavity working at LTE Band 13. First, a low-profile reference antenna element is chosen and structurally evolved using characteristic mode analysis (CMA) [11] to optimize against the expected angular-power spectrum (APS) of the incoming waves. The optimized element is then utilized in a quad-element setup that offers a suitable tradeoff between compactness and MIMO performance in terms of multiplexing efficiency [12]. The results show that the proposed hidden antenna solution outperforms a nonhidden solution of quad quarterwave-monopoles occupying the same lateral space. Moreover, for wideband operation, the proposed antenna element can be adapted to cover common low bands with frequencies 698-960 MHz.

II. Single-element Antenna Design

For the single-element antenna design, the 6 dB impedance bandwidth should cover LTE Band 13 (746-787 MHz), and it should fit into a typical car roof cavity with slanting walls (see Fig. 1(a) and 1(c)) [6], [9]. Furthermore, since LTE signals are exchanged with elevated base station antennas, the main directions of arrival (and departure) of the radio signals at the car roof tend to be uniformly spread in azimuth but cluster around $\theta = 60^{\circ}$–90° in elevation. This can be modeled by a 3D APS with uniform distribution in azimuth and truncated Gaussian distribution in elevation (see Fig. 1(b)) [13]. Therefore, the desired antenna pattern to match this outdoor channel's behavior is omni-directional over the azimuth plane and slightly raised from the ground plane, like that of a monopole antenna. However, to explicitly optimize the radiation pattern for the car channel, mean effective gain (MEG) [14] will be used to evaluate the overall channel gain for the given APS.

An inverted-F antenna (IFA) was used as the starting point for developing the hidden antenna solution, due to its low profile, monopole-like pattern and design simplicity. For convenience, the IFA in Fig. 2(a) was designed for the center frequency of 775 MHz. With this choice, the IFA's bandwidth

Manuscript received March 22, 2023, revised June 26, 2023 and July 31, 2023. This work was supported in part by the VINNOVA FFI programme (Dnr. 2014-01403).

Irfan Mehmood Yousaf was with Volvo Car Corporation, Sweden. He is with TE Connectivity, Sweden (E-mail: mehmoodirfan@gmail.com).

H. Aliakbari is with Volvo Car Corporation, Lund, Sweden and also with the Department of Electrical and Information Technology (EIT), Lund University, Lund, Sweden (E-mails: hanieh.aliakbariabar@volvocars.com).

B. K. Lau is with EIT, Lund University, 221 00 Lund, Sweden (E-mails: buon_kiong.lau@eit.lth.se).

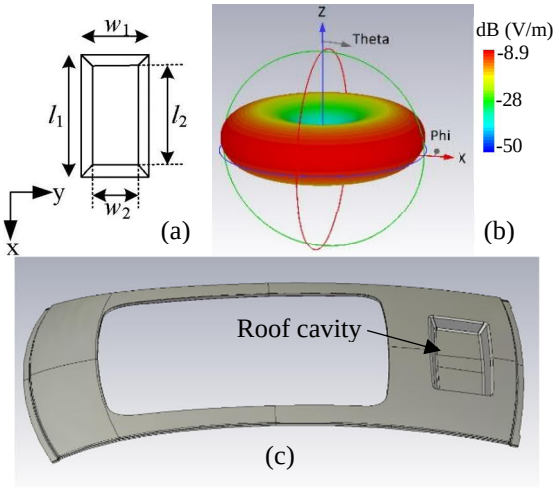

Fig. 1. (a) Dimensions of roof cavity on a ground plane, $w_1 = 220$ mm, $w_2 = 150$ mm, $l_1 = 570$ mm, $l_2 = 500$ mm. Cavity depth is 40 mm. (b) 3D APS of radio signals on car roof, where it is uniform distributed in azimuth and Gaussian distributed in elevation with mean of 75° and standard deviation of 15°. (c) Roof cavity for hidden antenna on a sedan car (Volvo S90) roof with sunroof.

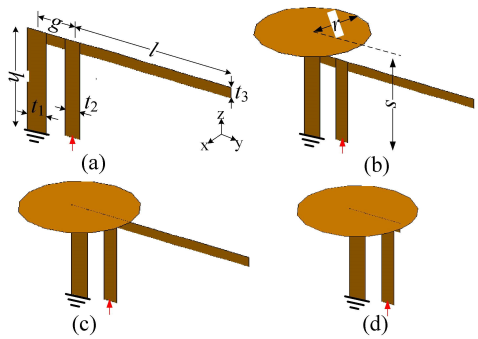

Fig. 2. Layout and parameters of the antenna on an infinite ground plane. h = 39 mm, t_1 = 8 mm, t_2 = 6 mm, g = 15 mm, t_3 = 4 mm, r = 24.5 mm, l = 65 mm. (a) IFA, (b) IFA with capacitive loading, (c) IFA with s = 39 mm, and (d) optimized IFA with l = 3 mm.

still covers the entire Band 13. The overall inverted-F arm (h + g + l) was set to be ~λ_0/4 at 775 MHz (λ_0 is the free space wavelength at 775 MHz). Its height h was optimized to give the needed bandwidth while not exceeding the cavity depth and g was optimized for the required matching. The IFA structure consists of infinitely thin PEC strips. CMA was performed on the IFA using 2019 Altair FEKO, with infinite ground plane, and Fig. 3 confirms that the lowest order mode is resonant at 775 MHz. The IFA on an infinite ground has a monopole-like pattern, but its null at θ = 0° is only suppressed in gain by ~5 dB. Moreover, in practice, the pattern will be even less monopolar when the IFA is placed in the cavity of Fig. 1(b), on a 1 m × 1 m (~2.5λ_0 × 2.5λ_0) ground plane. The finite ground and the cavity walls tilt the pattern upwards and the pattern null vanishes (see Fig. 4). Hence, the radiation pattern should be reshaped. Specifically, the MEG is optimized in the pattern shaping process for the propagation channel given by the APS.

One approach to decrease the gain in the vicinity of θ = 0° is to add a circular plate (or cap) of radius r above the centerline of the IFA's shorting strip (see Fig. 2(b)). The concept was first envisioned for application in an on-road RFID reader [15]. The cap is a form of capacitive loading, and the working principle

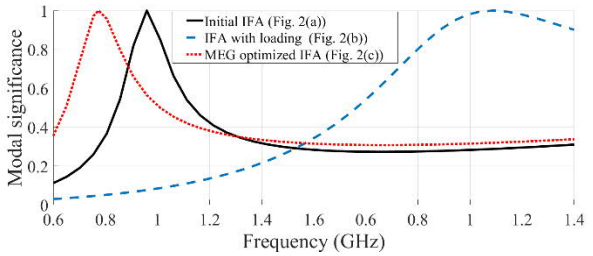

Fig. 3. Modal significance of original and evolved IFAs on infinite ground.

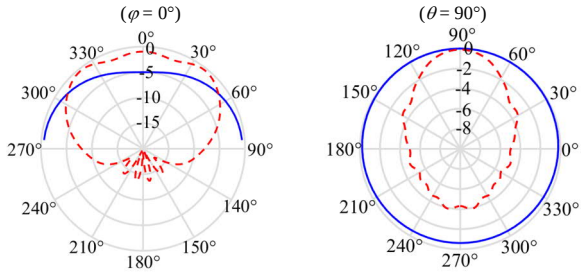

Fig. 4. Radiation patterns of the original IFA of Fig. 2(a) in two cuts, with infinite ground (—) or finite ground with cavity (---) at 775 MHz.

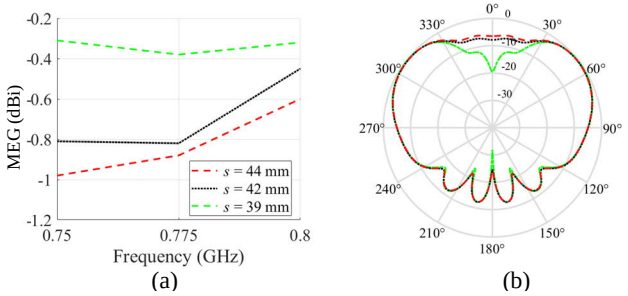

Fig. 5. (a) MEG for different heights of the disc from the finite ground plane, (b) Radiation pattern of the IFA in Fig. 2(b) in elevation (φ = 0° cut).

is that radiation from its induced current can be utilized to mitigate the IFA radiation at θ = 0°. It was optimized by its offset position (from above the shorting strip along the long arm) and radius to suppress the skyward radiation by 4 dB, while retaining the radiation efficiency and resonant frequency [15]. However, the effect of the height (s in Fig. 2(b)) is not presented in [15]. The specified height of 40 mm at 920 MHz translates to 47.5 mm at 775 MHz, which exceeds the roof cavity depth. Moreover, the work focuses on reducing the gain at θ = 0° and gives no explicit consideration to the channel.

Nevertheless, the circular cap addition provides a relatively simple approach to optimize the MEG of the IFA. The effect of the height s on the MEG is shown in Fig. 5(a), where the MEG increases with s, until the cap touches the top end of the IFA, with s = 39 mm (see Fig. 2(c)). The initial offset and radius r follow those of the reference design [15], but were found to have only little impact on MEG with the optimized s = 39 mm.

Figure 5(b) shows that the height of the capacitive loading does not influence the IFA's radiation pattern in the range θ = 45°–90°. However, the modal significance curve in Fig. 3 shows that the resonance frequency shifted down to 677 MHz for s = 39 mm (see Fig. 2(c)) due to the longer current path on the disk relative to having current only on the antenna's F-arm in Figs. 2(a) and 2(b). To restore the resonant frequency to 775 MHz, the IFA-arm length l was decreased to 3 mm (see Fig.

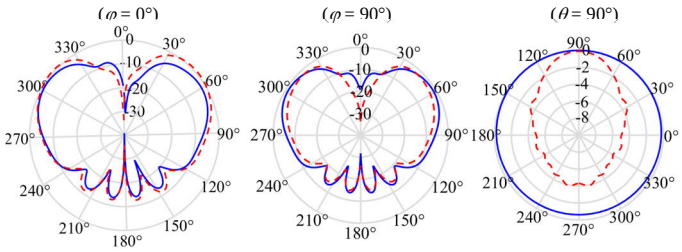

Fig. 6. Comparison of radiation patterns with (---) and without (—) cavity.

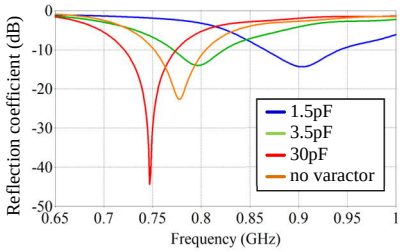

Fig. 7. Reflection coefficient of single-element without/with a series varactor.

2(d)). This also helped to reduce the size of the antenna for the later MIMO integration. It is noted that for s > 39 mm (i.e., no contact between the IFA and cap), shortening the F-arm will instead result in a higher resonant frequency. For example, with l = 3 mm, the resonant frequency shifts to 1.55 GHz (see Fig. 3).

Finally, the disc radius was re-optimized for matching, with no effect on the MEG, resulting in r = 24.5 mm. The simulated reflection coefficient is below −6 dB for 0.73-0.83 GHz. The dimensions of the optimized IFA are given in Fig. 2(d). Placing the optimized single antenna in Fig. 2(d) in the cavity center affected the radiation pattern (see Fig. 6) and the MEG slightly decreased by 0.4 dB. Optimizing the MEG for the cavity placement did not improve the MEG and it resulted in the same parameters values as for the no cavity case. It is noted that, if desired, a series varactor can be added to tune the single-element over the LTE low band of 698-960 MHz (see Fig. 7).

III. Multiple-element Antenna Configuration

Since the area of the considered cavity is relatively large, the quad elements of the MIMO antenna can be arranged in many configurations (i.e., by the element positions and orientations), including the three representative 1D and 2D configurations (Config. A, B, and C) depicted in Fig. 8. In general, a compact realization is preferred since the remaining space can then be utilized for other antennas or components. On the other hand, sufficient isolation and low correlation among the antenna elements is needed to achieve good MIMO performance. These two factors limit the minimum distance between the antenna elements. Moreover, due to the elements' asymmetric structure, the orientation can also be important. A further consideration is the limited cavity width of 150 mm at the base, where the corresponding cavity walls put an upper limit on the distance between the elements. This is because closer proximity to the walls changes capacitive coupling (hence impedance matching) as well as introduces distortion in the antenna element pattern. With these considerations in mind, the square arrays of Fig. 8 (Config. B and C) were studied in more detail. Multiplexing

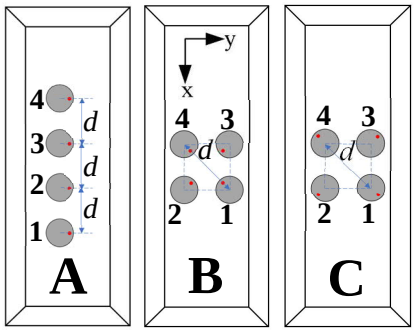

Fig. 8. Top view of Configurations A-C for the quad-element antenna in the cavity. The red dots indicate the feed locations.

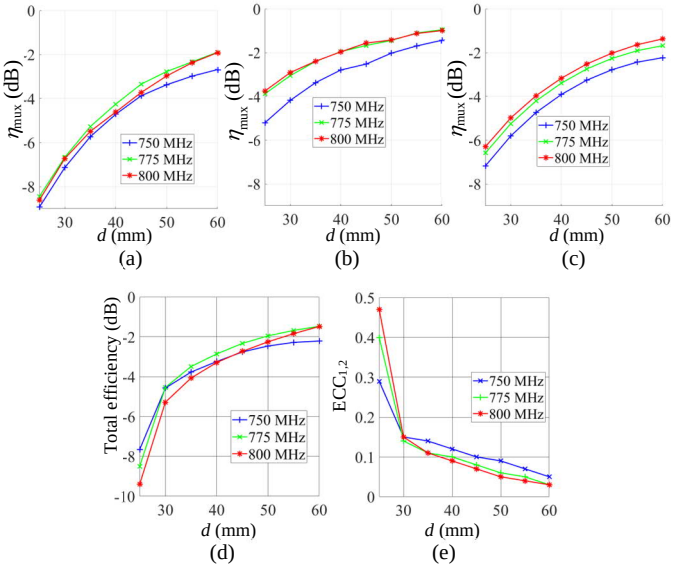

Fig. 9. Multiplexing efficiency η_{mux} vs. element distance d for Config. (a) B and (b) C in Fig. 8, and (c) quad quarterwave monopoles; (d) Total efficiency (same for all ports) vs. d and (e) ECC (ports 1 and 2) for Config. C.

efficiency η_{mux} [12], which captures MIMO system performance and generalizes the single-antenna concept of total efficiency for MIMO antennas, was used to find the best configuration for compact implementation, with each of the two configurations parametrized by the element distance d. In addition, the minimum element distance should be chosen to ensure a minimum isolation of 10 dB and a maximum magnitude of the complex correlation coefficient (CCC) of 0.4 (or maximum envelope correlation coefficient (ECC) of 0.16). Moreover, good matching, shown by sufficient 6 dB bandwidth, is also ensured for the range of element distance studied.

To calculate η_{mux} for Config. B and C over different d's (see Fig. 8), the total efficiencies of the quad elements and the radiation pattern based CCCs between all element pairs were obtained from the time-domain solver of 2020 CST Microwave Studio. Config. C offers significantly higher performance than Config. B (of up to 3 dB). However, the rate of increase in η_{mux} with d slows beyond 40 mm (i.e., saturation). For Config. C, further increase of distance from 40 mm to 60 mm will only yield less than 1 dB of performance gain, indicating that 40 mm is a good trade-off between performance and compactness of the proposed quad-element design. It is noted that the decreasing

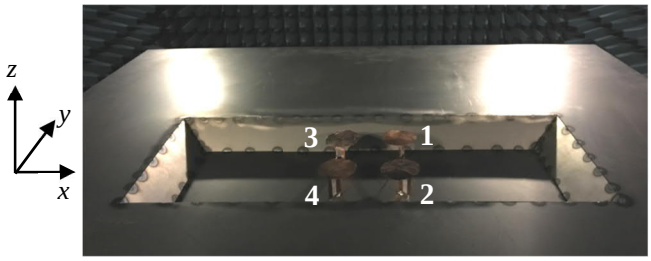

Fig. 10. Prototype of proposed quad-element MIMO antenna in Satimo SG-64.

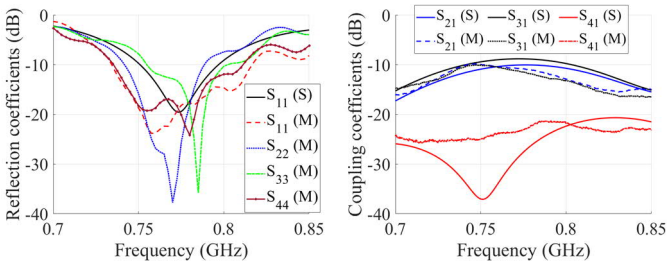

Fig. 11. Simulated (S) and measured (M) S-parameters of proposed quad-element MIMO antenna in cavity on a 1 m × 1 m ground plane.

η_{mux} with smaller d is due to increasing mutual coupling, which decreases the antenna elements' total efficiencies and generally increases ECCs (see Figs. 9(d)-9(e)) [12].

For benchmarking, the results for a quad-element setup with four quarterwave monopoles in the cavity (tuned to 775 MHz) were also obtained (see Fig. 9(c)). The monopoles are cylindrical PEC wires with the radius of 1 mm, and they were placed at the same positions as the feed points of the proposed array (Configuration C with d = 40 mm), to retain the same lateral array size. It is observed that the proposed array outperforms the reference monopole array, despite the nonhidden monopole array having more than twice the height of the proposed hidden quad-element array (i.e., 85 mm vs. 39 mm). For example, the multiplexing efficiency of the monopole array is -2.2 dB at 775 MHz as compared to -1.9 dB for the proposed hidden antenna solution.

IV. Measurement Results

The proposed quad-element array (Config. C with d = 40 mm) was fabricated in a cavity built using sheet metal that is normally used in the automotive industry (see Fig. 10). The ground plane dimensions were 1 m × 1 m. The antenna elements were made using thin (0.3 mm) copper plates. The scattering parameters were obtained with a 4-port vector network analyzer (see Fig. 11). Some results are omitted due to symmetry in the antenna structure, e.g., simulated reflection coefficients are identical for the four ports. The antenna pattern and efficiency were measured in a Satimo SG-64 system (see Fig. 10).

Both the simulated and measured reflection coefficients are better than −6 dB for 0.72-0.83 GHz (see Fig. 11). The simulated isolation between port 1 and the two beside it, i.e., ports 2 and 3, is ~10 dB (see the numbering of element/port in Fig. 8). The higher isolation between the elements across the diagonal (e.g., ports 1 and 4) is due to the larger distance between them. Simulated and measured antenna efficiencies and the MEGs are given in Table I. The simulated radiation

TABLE I
Total Efficiencies and MEGs for Given Channel (775 MHz)

	Efficiency (%)		MEG (dBi)	
Antenna #	Simulated	Measured	Simulated	Measured
1	72	82	-0.41	-0.30
2	72	80	-0.41	-0.19
3	72	81	-0.41	-0.24
4	72	81	-0.41	-0.20

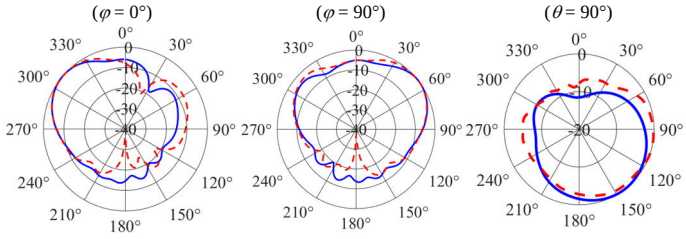

Fig. 12. Simulated (—) and measured (---) radiation patterns of port 2 of proposed quad-element antenna.

TABLE II
Simulated Envelope Correlation Coefficients (ECC) Among Ports 1-4 and Simulated/Measured Multiplexing Efficiency η_{mux}

Frequency (MHz)	$ECC_{1,2}$	$ECC_{1,3}$	$ECC_{1,4}$	Simulated η_{mux} (dB)	Measured η_{mux} (dB)
750	0.13	0.007	0.18	-2.8	-2.1
775	0.10	0.007	0.20	-1.9	-1.7
800	0.09	0.013	0.17	-1.9	-1.8

pattern of port 2 is shown in Fig. 12. Due to symmetry in this configuration, the pattern is only shown for one port. It can be seen that the maximum gain of each element is at θ = 50°. In addition, due to antenna coupling, the originally monopolar pattern of each element (see Fig. 6) becomes more directive in the azimuth plane, with the main beam pointing in orthogonal directions to those of other elements. The measured patterns are similar to the simulated patterns, but they are less directive and the patterns overlap more than the simulated ones. Simulated ECCs as well as simulated and measured multiplexing efficiency for the proposed antenna are given in Table II.

In general, the simulated and measured results agree with each other, and apart from measurement equipment tolerances, discrepancies can be attributed to the prototyping process, e.g., inaccuracies in the antenna dimensions, element placement and orientation, as well as imperfect soldering. In addition, discrete ports were used in the CST simulation model, as opposed to the SMA feed used in the prototype.

V. Conclusions

This work proposes a hidden antenna solution for a quad-element LTE antenna that is optimized for MIMO performance for the expected car channel properties. It has been found to offer competitive performance relative to a reference quad-monopole MIMO antenna that occupies the same footprint. Possible future work includes: 1) the extension of the antenna-channel optimization concept to design multiband or wideband elements and 2) the integration of the proposed MIMO antenna with other antennas in the roof cavity.

REFERENCES

[1] E. Dahlman, S. Parkvall, and J. Skold. *5G NR: The Next Generation Wireless Access Technology*. 2nd ed. London: Academic Press, 2020.

[2] N. Guan, H. Tayama, M. Ueyama, Y. Yoshijima, and H. Chiba, "A roof automobile module for LTE-MIMO antennas," in *Proc. IEEE-APS Topical Conf. Antennas Propag. Wireless Commun. (APWC' 2015)*, Turin, Italy, Sep. 7-11, 2015, pp. 387-391.

[3] A. Thiel, L. Ekiz, O. Klemp, and M. Schultz, "Automotive grade MIMO antenna setup and performance evaluation for LTE-communications," in *Proc. IEEE Int. Workshop Antenna Technol.*, Karlsruhe, Germany, Mar. 4-6, 2013, pp.171–174.

[4] Y. Liu, Z. Ai, G. Liu, and Y. Jia, "An integrated shark-fin antenna for MIMO-LTE, FM, and GPS applications," *IEEE Antennas and Wireless Propag. Letters*, vol. 18, no. 8, pp. 1666-1670, Aug. 2019.

[5] L. Low, R. Langley, R. Breden, and P. Callaghan, "Hidden automotive antenna performance and simulation," *IEEE Trans. Antennas Propag.*, vol. 54, no. 12, pp. 3707-3712, Dec. 2006.

[6] G. Artner, R. Langwieser, and C. F. Mecklenbräuker, "Concealed CFRP vehicle chassis antenna cavity," *IEEE Antennas and Wireless Propag. Letters*, vol. 16, pp. 1415-1418, 2017.

[7] N. Guan, H. Chiba, Y. Yamaguchi, Y. Niihara, and H. Tayama, "A flat roof automobile antenna module for LTE, GPS and SDARS applications," in *Proc. IEEE-APS Topical Conf. Antennas Propag. Wireless Commun. (APWC'2014)*, Palm Beach, FL, Aug. 3-9, 2014, pp. 11-14.

[8] N. Guan, H. Tayama, M. Ueyama, Y. Yamaguchi, and H. Chiba, "An invisible vehicle roof antenna," in *Proc. IEEE-APS Topical Conf. Antennas Propag. Wireless Commun. (APWC'2016)*, Cairns, Australia, Sep. 19-23, 2016, pp. 51-54.

[9] I. M. Yousaf and B. K. Lau, "On performance of hidden car roof antennas," in *Proc. 12th Europ. Conf. Antennas Propag. (EuCAP)*, London, United Kingdom, Apr. 9-13, 2018.

[10] L. Y. Nie, X. Q. Lin, J. Y. Chen, J. Zhang, B. Wang, Z. Q. Yang, and Y. Fang, "A low-profile coplanar dual-polarized and dual-band base station antenna array," *IEEE Trans. Antennas Propag.*, vol. 66, no. 12, pp. 6921-6929, Dec. 2018.

[11] B. K. Lau, M. Capek, and A. Hassan, "Characteristic modes – progress, overview, and emerging topics," *IEEE Antennas Propag. Mag.*, vol. 64, no. 2, pp. 15-22, Apr. 2022.

[12] R. Tian, B. K. Lau and Z. Ying, "Multiplexing efficiency of MIMO antennas," *IEEE Antennas Wireless Propag. Lett*., vol. 10, pp. 183-186, 2011.

[13] Z. Ying and V. Plicanic, "Characterization of multi-channel antenna performance for mobile terminal by using near field and far field parameters," in *COST 273*, TD (04) 095, Goteborg, Sweden, Jun. 2004.

[14] T. Taga, "Analysis for mean effective gain of mobile antennas in land mobile radio environments," *IEEE Trans. Veh. Technol*., vol. VT-39, no. 2, pp. 117–131, May 1990.

[15] Y. Wang, A. J. Pretorius, and A. M. Abbosh, "Low-profile antenna with elevated toroid-shaped radiation for on-road reader of RFID-enabled vehicle registration plate," *IEEE Trans. Antennas Propag.*,vol. 64, no. 4, pp. 1520–1525, Apr. 2016.